ADVANCED MATERIALS
www.advmat.de

Theoretical Study of Piezo-phototronic Nano-LEDs

*Ying Liu, Simiao Niu, Qing Yang, Benjamin D. B. Klein, Yu Sheng Zhou, and Zhong Lin Wang**

The piezo-phototronic effect is due to the presence of piezoelectric charges at material interfaces, and may be utilized to control carrier generation, transport, separation and/or recombination, thereby improving the performance of optoelectronic devices.[2] The performance of such devices can be tuned by applying external mechanical stress/strain, which gives rise to new scientific phenomena and technological applications. Many reports have detailed observations of the piezo-phototronic effect and its impact on optoelectronic processes, including significant responsivity enhancement in photodetection,[3] output optimization of photocells,[4] improvement of solar-cell efficiency,[5] and most importantly, enhancement of the light-emission efficiency of inorganic light-emitting diodes (LEDs) and inorganic/organic hybrid LEDs.[1,6–8] An analytical model has also been proposed for the piezo-phototronic effect in metal–semiconductor structures.[9] Such theoretical calculations and numerical modeling not only help to understand basic physics of the effect, but also provide guidance for device design and optimization. However, previous explanations of this effect were limited to 1D analyses, which did not take device geometry factors into consideration, especially in light-emitting devices. Here, we have developed a methodology for 2D simulation of the piezo-phototronic effect in a p–n-junction-based LED. With this methodology, we utilize the finite-element method (FEM) to overcome the difficulties of analytical modeling and provide more-intuitive results, including band-structure and device current characteristics under different device geometries, which can be compared with experimental data and provide an optimization approach.

Y. Liu,[+] S. Niu,[+] Y. S. Zhou, Z. L. Wang
School of Material Science and Engineering
Georgia Institute of Technology
Atlanta, Georgia 30332–0245, USA
E-mail: zlwang@gatech.edu

Q. Yang
State Key Laboratory of Modern Optical Instrumentation
Department of Optical Engineering
Zhejiang University
Hangzhou 310027, China

B. D. B. Klein
School of Electrical and Computer Engineering
Georgia Institute of Technology
Atlanta, Georgia GA 30332–0250, USA

Z. L. Wang
Beijing Institute of Nanoenergy and Nanosystems
Chinese Academy of Sciences
Beijing, China

[+]These authors contributed equally to this work.

DOI: 10.1002/adma.201402328

A critical concept in the piezo-phototronics effect is the formation of a channel induced by piezo-charge in the p–n junction depletion region, which can serve as an effective means of tuning the carrier separation or recombination. For the LED structure, a positive charge channel is proposed, for trapping the holes in the valence band at the metallurgical junction and increasing the recombination probability,[2] so that the light-emission efficiency is enhanced. Therefore, our objective here is to validate the existence of such a charge channel from rigorous theoretical calculation.

To address this problem, as the first step, we need to get the piezo-charge density at the p–n junction interface. The piezo-charge density can be obtained from the piezoelectric polarization P, which can be retrieved from the constitutive equation, as shown below:[10]

$$P_i = \mathbf{e}_{ijk}\boldsymbol{\varepsilon}_{jk} = \rho_{\text{piezo}} W_{\text{piezo}} \tag{1}$$

where $\boldsymbol{e}_{ijk}$ is the matrix of piezoelectric constants, $\boldsymbol{\varepsilon}_{jk}$ is the strain tensor, ρ_{piezo} is the density of the induced piezo-charges, and W_{piezo} is the width of the spatial distribution of the piezo-charges at the material interface, which is assumed to be much smaller than the width of the charge-depletion zone around the p–n junction. In this simulation, P is first calculated for the piezoelectric material by assuming that it is an insulator, and then the obtained polarization charges at the interface area are used as an input for the next step of the calculation.

Then, using a 1D finite-element model, we have calculated the band-edge deformation under different strain conditions, and the resulting conduction band is shown in **Figure 1**b for a homojunction. The spatial variation of the valence band edge is identical to the spatial variation of the conduction band (offset by the bandgap energy), and thus it is not necessary to plot it for the homojunction. The deformation of the valence band edge and the conduction band edge are calculated by solving the Poisson equation.[11] In COMSOL, the electron concentration n and hole concentration p are solved self-consistently in the depletion region.

In regions far from the depletion zone, the conduction band energy and valence band energy are flat and fixed at values calculated from the bulk material properties and the background doping profile. Therefore, the built-in potential ψ_{bi} is fixed at the difference between the Fermi levels of the original doping. When piezo-charges are present, a 1D approximation will result in:

$$N_A W_{\text{Dp}} = N_D W_{\text{Dn}} + \rho_{\text{piezo}} W_{\text{piezo}} \tag{2}$$

N_A is the p-type doping density in the p-type region, N_D is the n-type doping density in the n-type region, W_{Dp} is the depletion

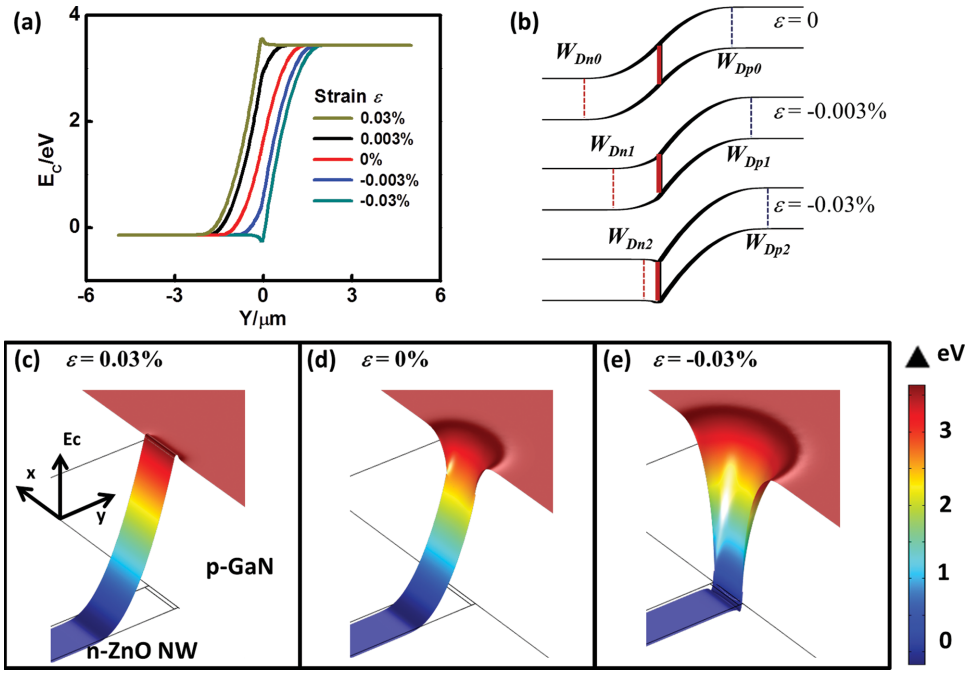

Figure 1. a) Conduction band deformation of n-ZnO/p-ZnO structure under different strains on the n-type side, 1D simulation. b) Illustration of the formation of charge channel. c–e) Conduction band in height expressed from 2D simulation in n-ZnO/p-ZnO structure under: c) 0.03% strain, d) no strain, and e) –0.03% strain at the n-type side.

width in the p-type region, and W_{Dn} is the depletion width in the n-type region.

Thus, the depletion region will shrink on the n-type side and expand on the p-type side when $\rho_{piezo} > 0$ (positive piezo-charges), as shown in Figure 1a at strain $\varepsilon = -0.003\%$; when $\rho_{piezo} < 0$ (negative piezo-charges), the depletion region will expand on the n-type side and shrink on the p-type side, as shown in Figure 1a at $\varepsilon = +0.003\%$. In previous analytical models, it was assumed that the depletion region will have negligible change in width under strain, and the influence of piezo-charges is mainly changing the local built-in potential. As both the density and total amount of piezo-charges are dependent only on piezoelectric coefficient of the material and the existing strain, and independent of the doping profile of the material, this assumption is valid when the doping profile is low so that the total amount of depletion charges of the unstrained structure is far greater than the total amount of piezo-charges. Referring to experiments, this assumption is applicable to hydrothermally grown NWs with abundant defects as well as photodetectors and solar cells with photoexcited free charge carriers,[5,12] as the depletion-charge amount in these materials is far larger than that of piezo-charges under experimental straining conditions. However, in our simulation, the doping profile is low, such that the total amount of intrinsic depletion charge is much smaller than the amount of piezo-charges at the junction interface. Thus the presence of piezo-charges at the interface results in a significant change to the width and shape of the depletion zone due to the electrostatic interaction of the piezo-charges with the carriers in the region.

When the total amount of piezo-charges further increases and $\rho_{piezo} W_{piezo} >> N_D W_{Dn}$, as shown in Figure 1b, the entire depletion region shifts toward the p-type region; in such a case W_{Dn} shrinks to the width of the piezo-charges distribution, and the localized piezo-charges will affect the charge redistribution, and we have $\Psi_n + \Psi_p > \Psi_{bi}$, where Ψ_n is the potential built in the n-type side and Ψ_p is the potential built in the p-type side. Thus, in the depletion region, the local deformation will result in the presence of a charge channel, i.e., electron traps at $\varepsilon = -0.03\%$ and hole traps at $\varepsilon = +0.03\%$ shown in Figure 1a.

Next, the 2D geometry in **Figure 2**a was simulated, in which case the Poisson equation is:

$$\left\{ \varepsilon_r \left(\frac{\partial E_x}{\partial x} + \frac{\partial E_y}{\partial y} \right) = -qN_A \quad \frac{\partial^2 \Psi_i}{\partial x^2} + \frac{\partial^2 \Psi_i}{\partial y^2} = \frac{qN_A}{\varepsilon_r} \right. \quad \text{on p-side depletion region} \quad (3a)$$

$$\left\{ \varepsilon_r \left(\frac{\partial E_x}{\partial x} + \frac{\partial E_y}{\partial y} \right) = qN_D \quad \frac{\partial^2 \Psi_i}{\partial x^2} + \frac{\partial^2 \Psi_i}{\partial y^2} = -\frac{qN_D}{\varepsilon_r} \right. \quad \text{on n-side depletion region} \quad (3b)$$

$$\left\{ \varepsilon_r \left(\frac{\partial E_x}{\partial x} + \frac{\partial E_y}{\partial y} \right) = q\rho_{piezo} \quad \frac{\partial^2 \Psi_i}{\partial x^2} + \frac{\partial^2 \Psi_i}{\partial y^2} = -\frac{q\rho_{piezo}}{\varepsilon_r} \right. \quad \text{in piezo-charge region} \quad (3c)$$

2D height plots are shown in Figure 1c–e to demonstrate the change in conduction band structure in the 2D case. In the simulated geometry, in regions close to the middle line on the y-axis, $\frac{\partial E_y}{\partial y}$ and $\frac{\partial^2 \Psi_{bi}}{\partial y^2}$ will be close to zero, and the result is similar to the 1D result. In other parts of the depletion zone, the influence of the piezo-charges will decrease compared to that in the 1D simulation, which means that the charge channels will require greater strain to become significant.

The current–voltage characteristics are among the most important data for piezotronics and piezo-phototronics. The

Adv. Mater. 2014,
DOI: 10.1002/adma.201402328

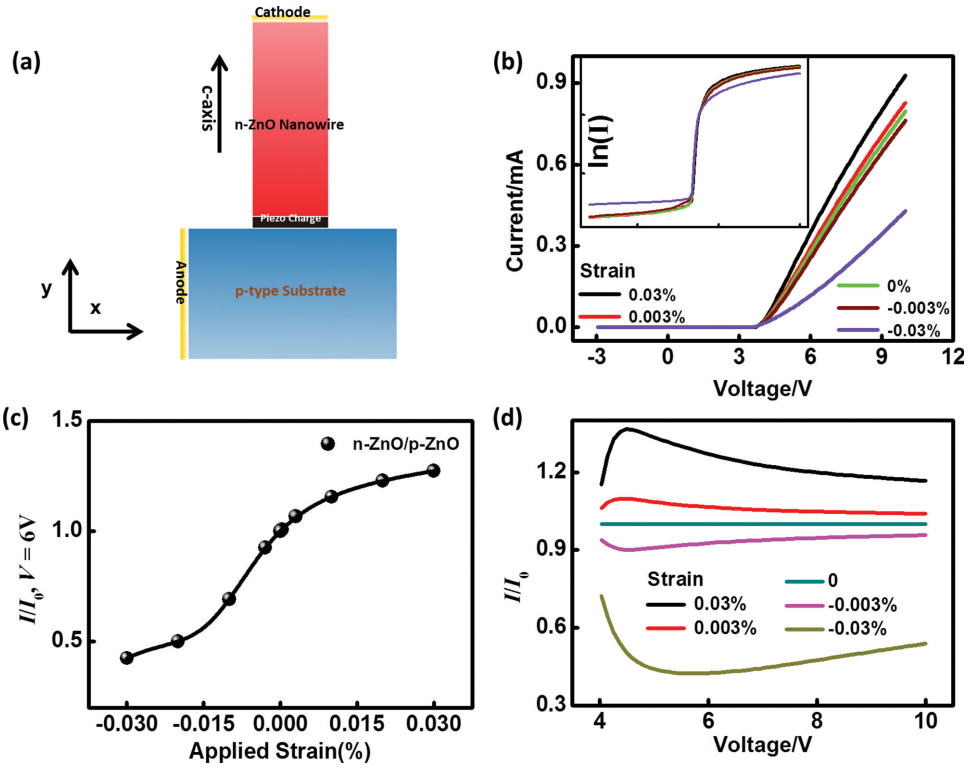

Figure 2. a) Geometry of 2D simulation. b) Current–voltage curve of n-ZnO/p-ZnO. c) Change of current when bias is fixed at 6 V under different strain, I_{strain}/I_0 vs ε. d) Relative change of current under strain vs applied voltage, I_{strain}/I_0 vs V.

simulation results for n-ZnO/p-ZnO structure with the geometry layout shown in Figure 2a are plotted in Figure 2.

For current calculation and integration through the whole geometric structure, the time-dependent continuity equations for current density are used:[11]

$$\frac{\partial n}{\partial t} = -\frac{1}{q}\nabla \cdot \vec{J}_n - U_n + G_n \tag{4a}$$

$$\frac{\partial p}{\partial t} = \frac{1}{q}\nabla \cdot \vec{J}_p - U_p + G_p \tag{4b}$$

In the drift-diffusion approximation we have:

$$\vec{J}_n = \mu_n n \nabla E_C + qD_n \nabla n|_{W_{Dn}} \tag{4c}$$

$$\vec{J}_p = \mu_p p \nabla E_V - qD_p \nabla p|_{W_{Dp}} \tag{4d}$$

where J_n and J_p are electron and hole current densities; U_n and U_p are electron and hole recombination rates; G_n and G_p are electron and hole generation rates, E_C and E_V are conduction band energy and valence band energy; q is the electron charge; and D_n and D_p are electron and hole diffusion coefficients, respectively. The series resistance is set as zero for simplicity.

The depletion region is the main barrier to the device current; however, the undepleted p-doped substrate region provides a large effective series resistance, due to the low mobility of the majority holes. When compressive strain is applied to the device, the p-type depletion region increases in area and spreads out to form a semicircle in the substrate. Current will be injected into the substrate along the entire boundary of the depletion region and travel to the substrate contact, as has been confirmed by plots of the current density. As the radius of the semicircular depletion boundary increases, the current must travel a larger average distance from injection to the contact due to the contribution of current streamlines injected on the side of the semicircle opposite the contact side, thereby increasing the effective series resistance of the substrate and decreasing the device current. When tensile strain is applied, the p-type depletion region shrinks and the n-type depletion region enlarges, shrinking the depletion region boundary to the diameter of the nanowire, and lowering the effective series resistance of the substrate. In support of this proposed mechanism, comparison simulations are also provided in the Supporting Information (Figure S1), showing that when hole mobility is artificially increased to a high value, the influence of strain on current will greatly diminish. Even though the change is related to a series of resistors, it is totally different from piezoresistance effect and contact area effect, as the change of resistance and current comes from the change of depletion area caused by the introduction of piezo-charges. The above analysis is consistent to the result shown in Figure 2b, where

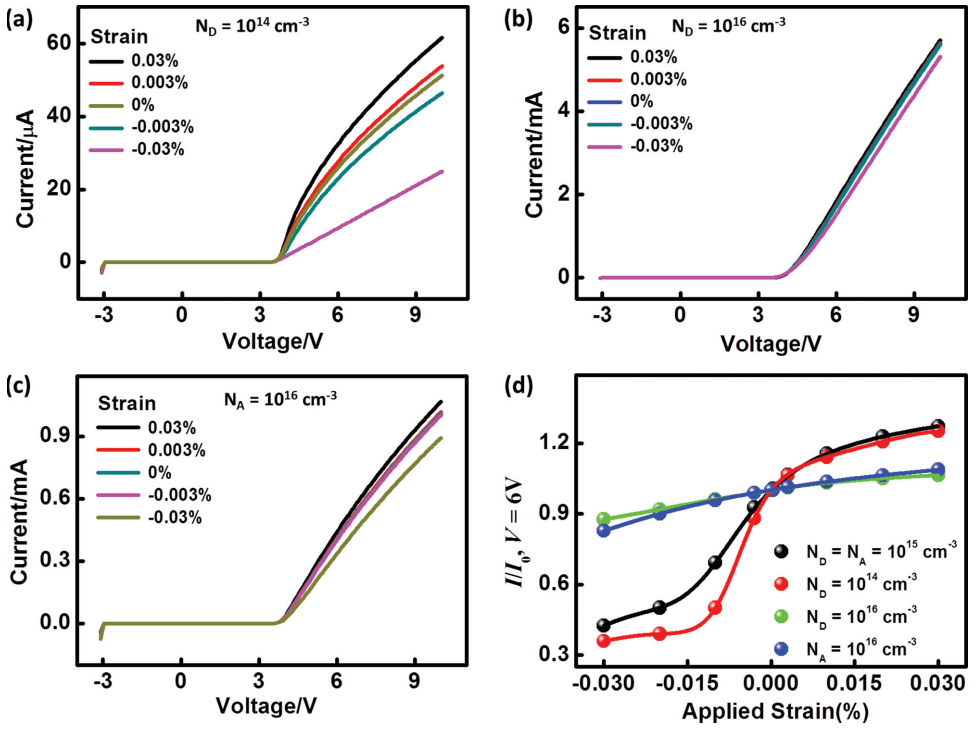

Figure 3. Current–voltage simulation result from: a) N_D changes to 10^{14} cm^{-3}, b) N_D changes to 10^{16} cm^{-3}, c) N_A changes to 10^{16} cm^{-3}. d) Comparison of calculated current at a fixed bias of 6 V for different doping concentrations by normalizing to the result received for $N_D = N_A = 10^{15}$ cm^{-3}.

the *I*–*V* curves under different straining conditions are plotted. A monotonic increase in current with increasing tensile strain and decreasing compressive strain is clearly shown. For more intuitive understanding, the current at 6 V under each straining condition are plotted into one curve in Figure 2c. It is easy to conclude that under lower strain, the current changes almost exponentially with strain; however, under higher strain, the current will saturate when p-channel or n-channel forms at the interface. Another comparison is made for the relative change in current I_{strain}/I_0 under different bias voltage for each strain condition, as listed in Figure 2d. The value of I_{strain}/I_0 at any strain first increases quickly with V, and when V gets higher, I_{strain}/I_0 tends to slightly decrease with V, and finally saturates. When V and ε are small, the trend of I_{strain}/I_0 vs V and I_{strain}/I_0 vs ε are close to exponential, these results agree well with our previous analytical models in which exponential relationships between I_{strain}/I_0 vs V and I_{strain}/I_0 vs ε were predicted.[9] When V and ε get larger, the I_{strain}/I_0 vs $V$and I_{strain}/I_0 vs ε are closer to linear, which also suggests the effect of series resistance as well as other non-ideal factors.

Based on the simulation of the device current, we then controlled the parameters related to device design and studied the optimization of the piezo-phototronics effect using a numerical method.

The doping profile of both the NW and the substrate is usually coupled with geometric factors and is an essential factor in device design. In the above sample simulation, the doping profile is set at a relatively low level. Simulating different doping profiles can help us compare the piezo-phototronics effect in materials synthesized by different methods. Several sets of simulations have been conducted to study the influence of doping.

Figure 3a–c show the $I - V$ curves under different strain conditions when the doping profile is changed. Figure 3d plots the relative change of current I_{strain}/I_0 at 6 V bias under different strains for these simulations together for easier comparison. Similar to the conclusion we provided in the simulation above, applying tensile strain can still enhance the current under all of these conditions, but the extent of enhancement varies with the different doping profiles. Generally, when the doping profile increases, the relative impact of the piezo-phototronic effect decreases; and when doping profile decreases, the impact of the piezo-phototronic effect increases. This is because the lower the doping profile, the greater the magnitude of the piezo-charge is relative to depletion charges, and the more significant the piezo-phototronics effect. This result can help explain the attenuation of piezo-phototronics effect in photodetection experiments with the increase of the detected light intensity.[3,9,13] When the intensity of the detected light increases, the electron–hole pairs generated can overwhelm the influence of piezo-charges.

When the substrate doping reduces to 10^{14} cm^{-3} while the NW doping stays the same, the trend of I_{strain}/I_0 under different strains becomes unsteady, as shown in Figure S3 in the Supporting Information. The reason for such behavior is multifold. When the substrate doping is small, the depletion region on the p-type side will be relatively large in size. In 1D calculation under strain-free conditions, decreasing the doping profile to 10% of original value results in a depletion region that is 10-times larger. In 2D simulation, the change of depletion region profile varies in multiple directions. In the direction perpendicular to material interface, the change of depletion region is close to the change in 1D simulation; and along the direction parallel to material interface, the change of depletion region is

Adv. Mater. **2014**,
DOI: 10.1002/adma.201402328

smaller than that in 1D simulation. When the p-type depletion region is large enough to interact with the electrode, it may be cut off in the electrode area, and influence of piezo-charges on band structure is much more complicated than previous simulation conditions. Therefore, the device current will also be influenced by both change in band structure and the inner resistance created within the depletion region and become unsteady.[14] Moreover, the doping profile will also influence the band alignment in the p–n junction by changing the Fermi level. Considering the case of ZnO, the change in doping profile does not have a strong effect on the formation of charge channels; however, in a non-degenerate semiconductor, this change could be significant.

This result supports the idea that the piezo-phototronics effect is optimized at certain doping profiles that are neither too high nor too low. The specific optimized value is also related to material properties.

In bulk materials, the device size is orders of magnitude greater than the depletion width, and the electrode outlet is usually far away from the depletion region, the size or geometric layout usually influences the device performance only by influencing the equalized series resistance of the material. However, in the study of NW devices of microsized structures, the size of the devices could easily be comparable to the size of the depletion region, and thus their performance can be easily affected by geometry size. For example, when the geometry size is small, the depletion region may either be confined in the geometry in certain dimensions, or may overlap with the electrodes.

Simulation results with change of either the NW diameter or the substrate size are demonstrated in **Figure 4**. In Figure 4a, the substrate size in the simulation was cut half in length and half in width for the structure, which means that the substrate size is 5 μm × 5 μm. From comparison with the original model, the relative current change at the same strain of the small device structure is about 20% larger than that of the original structure for all straining conditions. This kind of uniform enhancement under all strain conditions means that as far as the simulated strain and applied voltage is concerned, the depletion region does not overlap with the electrodes and induce unsteadiness in current behavior, and such a shrink in size has mainly changed the series resistance.

Figure 4b has set the NW diameter to 2 μm and Figure 4c has set the NW diameter in half to 500 nm. The overall comparison of R value for these two structures with the original geometry is shown in Figure 4d. Besides inner resistance, this change also comes from the fact that, in direction parallel to material interface (x-direction), the change of band structure by strain is weaker than the change perpendicular to material's interface (y-direction), and thus the thinner the NW, the stronger overall the piezo-phototronics effect. For verification, in Figure 4e we have plotted the E_C value under different strains for different points along the direction parallel to material interface (x-direction); the y values for these points are in the middle of the piezo-charge distribution area. From an optimization aspect, as ZnO is non-ferroelectric, there is no such concept of domains as in PZT or $BaTiO_3$,[15,16] and as long as the NW size is larger than a few crystal lattices, a smaller NW will give a stronger piezo-phototronics effect. Smaller NW sizes corresponding to NW LED array experiments are also simulated, and the results are shown in the Supporting Information (Figure S5).

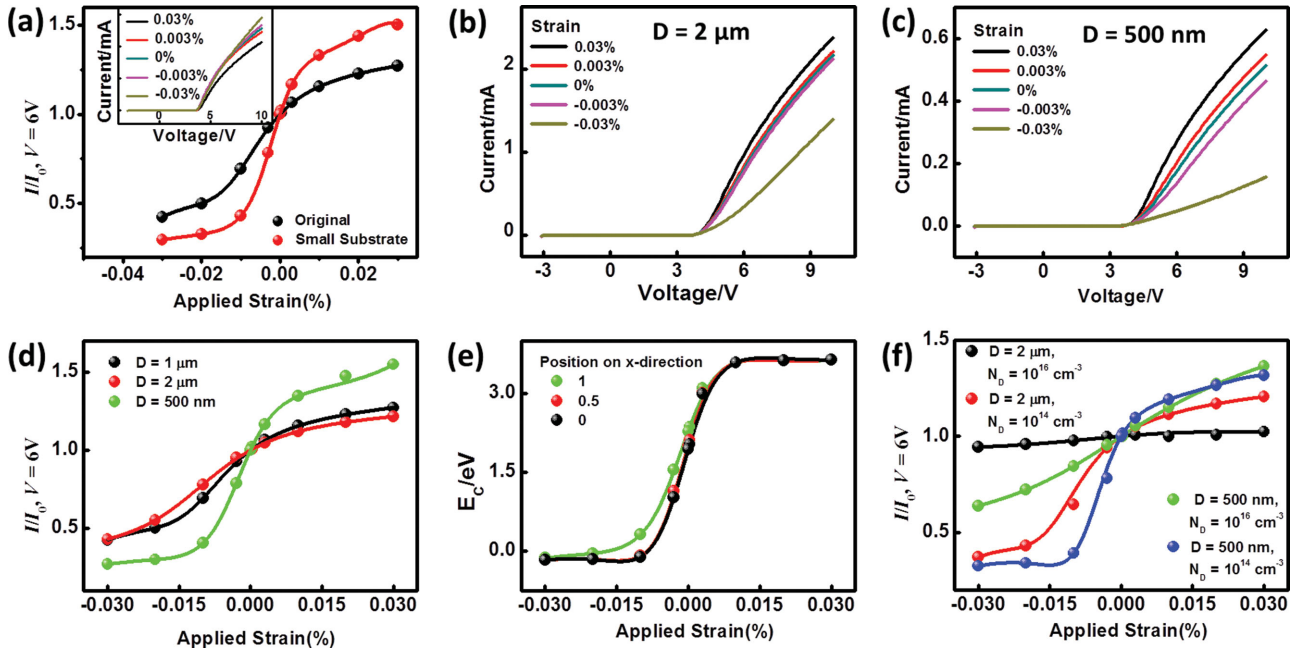

Figure 4. a) Comparison of n-ZnO/p-ZnO with smaller substrate of size 5 μm × 5 μm and result in Figure 2, I_{strain}/I_0 vs ε at 6 V bias; the inset is the current–voltage characteristics of such a simulation. b) Current–voltage characteristics of n-ZnO/p-ZnO with NW diameter D = 2 μm. c) Current–voltage characteristics of n-ZnO/p-ZnO with NW diameter D = 500 nm. d) Comparison of I_{strain}/I_0 vs V, between (b) and (c) with Figure 2c. e) The E_C value under different strain for different locations along the direction parallel to material interface; the position along the x-direction is counted from the middle point in the piezo-charge distribution area. f) Relative change of current under different NW size and NW doping.

Table 1. Material properties used in simulations.

Property	ZnO	GaN
Relative Permittivity [ε_r]	9.1	10
Bandgap (E_g) [eV]	3.38	3.40
Electron Affinity (χ) [eV]	4.5	4.1
Valence band density of states (N_V) [cm^{-3}]	3.5×10^{18}	4.1×10^{19}
Conduction band density of States (N_C) [cm^{-3}]	1×10^{20}	1.2×10^{18}
Electron Mobility (μ_n) [$m^2\ V^{-1}\ s^{-1}$]	0.2	0.2
Hole Mobility (μ_p) [$m^2\ V^{-1}\ s^{-1}$]	10^{-3}	10^{-3}

As a further step, a plot of the coupling of geometry size and doping profile is given in Figure 4f. Four lines were plotted, each featuring a different NW size and different NW doping. Lower NW doping and a smaller NW size can both enhance the piezo-phototronics effect, yet their influence has a minor difference. Lower NW doping results in a faster enhancement under lower strain, and the current saturates faster. A smaller NW size results in a more uniform change over the range of strain values.

In optoelectronic devices, heterojunctions are usually utilized to eliminate minority carrier injection and minimize photon reabsorption.[17] As far as band structure is concerned, the major difference between heterojunction and homojunction lies in the discontinuity formed in the interface between different materials and the associated band mismatch. This band discontinuity could provide an additional charge potential barrier depending on the materials used. Plus, heterojunctions can provide larger reflection in the material interface and is favored in LED fabrications. In the case of piezo-phototronics effect, piezo-charges can help either "recover" or enhance the discontinuity by tuning the local band structure.

Here, we compare the n-ZnO NW/p-GaN structure with the n-ZnO/p-ZnO structure studied earlier to examine the influence of different types of junctions on the optimization of the piezo-phototronics effect. From **Table 1**, the bandgaps of ZnO and GaN are similar, leaving similar discontinuities in both the valance band and the conduction band, which simplifies the comparison of the simulation results. For a simpler comparison and more-intuitive perspective, the result for 1D calculation for heterojunction is shown in **Figure 5**a and 5b for conduction band and valence band as comparison for Figure 1a. From band structure calculation, the deformation under different strain is similar to the results for a homojunction. In calculation of the device current, the case is much more complicated, as parameters such as charge-carrier mobility and diffusion constants can be totally different in various materials under various doping condition, and discussion regarding different carrier mobility is too complicated and beyond the scope of this paper. For simpler comparison, a simulation setting the charge carrier mobility as the same value in GaN is performed, and the results are shown in Figure 5c and 5d. Figure 5c shows that the *I–V* curve under different strain conditions is almost identical to that of a homojunction. The curves for current under 6 V bias voltage but under different strain conditions are plotted together with that of homojunction in Figure 5d, which shows the impact of piezo-phototronics effect is slightly stronger in a homojunction than in a heterojunction, especially when compressive strain is applied, without considering the advantages of heterojunction in optoelectronics or the differences in charge mobility and lifetime between various materials. From previous discussions and comparison simulations displayed in Figure S1 and Figure S2 in the Supporting Information, a lower hole mobility on the p-type side is also desired for the piezo-phototronics effect.

We have also performed simulation using material set up and geometry layout used in previous experiments,[1,7] and the results are found in Figure S6 in the Supporting Information. From the results, we have confirmed that the geometry layouts used in these experiments can also effectively display the piezo-phototronics effect, but these designs can be further optimized according to the methods provided here.

In conclusion, we report a methodology for numerically simulate the piezo-phototronics effect in nano LEDs for both 1D structure and 2D structure. By studying the change of band structure, we have confirmed the shift of depletion region and formation of charge channel at the interface with application of a proper amount of mechanical strain, which has been proposed in previous experimental reports as the major mechanism for the gigantic increase of emission efficiency of LED. By simulating the current characteristics of 2D devices, we have studied the factors including doping profile, geometric factors and material considerations and their influence on the piezo-phototronics effect. We have found that lower NW doping and smaller NW size are favorable for application in piezo-phototronic nano LEDs, and without considering sophisticated factors like charge mobility, homojunctions are potentially more favorable than heterojunctions for improved piezo-phototronic effect.

In conclusion, our methodology has validated previous reported data, and can provide an optimization strategy for future experimental design of piezo-phototronic research. For future perspectives, using this methodology, it is also possible to simulate the kinetics of the transient process of piezo-phototronics effect, where the applying/releasing of the strain influences the accumulation/disappearance of the piezo-charges. Beyond Nano-LEDs, our methodology can also be expanded to other types of devices based on the p–n junction, such as photodetectors and solar cells.

Model Development

COMSOL Multiphysics software was utilized for most of the calculations in this study. A major difficulty with semiconductor device simulation via the FEM is the large gradient of charge concentration, electric field and local band energy in the depletion region, which may result in singularity or failure to converge. Thus, in our simulation, higher order solvers and mesh refinement were utilized. For carrier-current calculations, both the time-dependent solver and stationary solver were used in conjunction with the introduction of electrical circuit equations in the COMSOL.

The two-dimensional layout of our theoretical model was built according to common experimental designs,[7,18] which includes an n-type piezoelectric nanowire (NW) structure and a thin-film p-type substrate, as shown in Figure 2a. The NW

Adv. Mater. **2014**,
DOI: 10.1002/adma.201402328

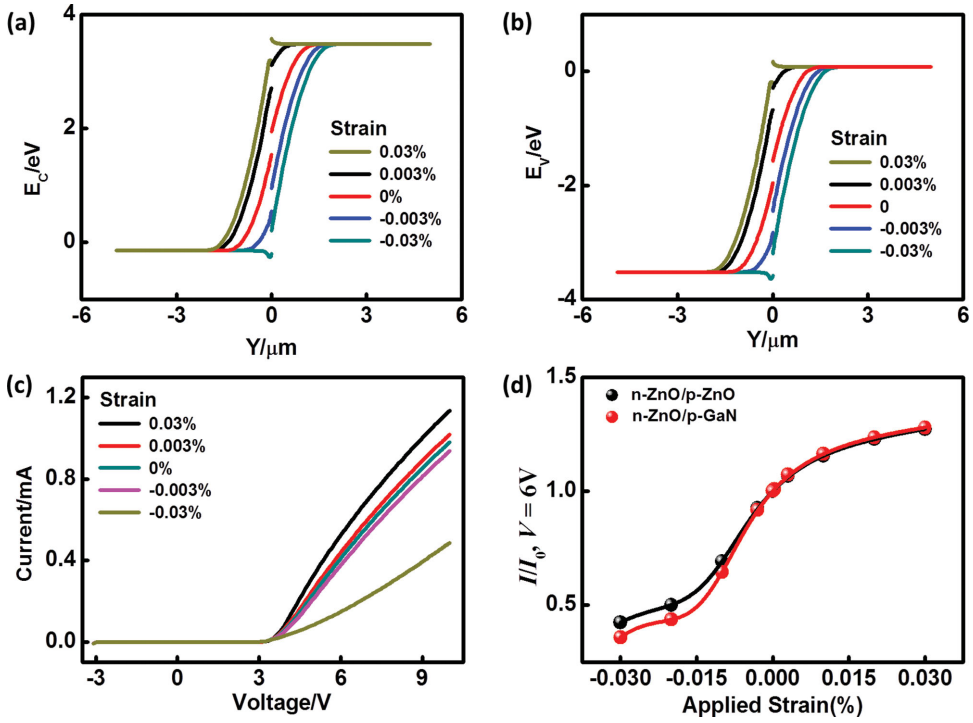

Figure 5. Simulation results for n-ZnO NW/p-GaN substrate structure. a) Conduction band deformation of such structure under different strain at n-type side base on 1D simulation, which is chosen for comparison purpose. b) Valence band deformation of such structure under different strain at n-type side based on 1D simulation. c) Current–voltage characteristics based on 2D simulation: geometry layout and doping are set as the same value as in Figure 2a. d) I_{strain}/I_0 vs ε and comparison with Figure 2b.

is 1 μm × 10 μm and the substrate is 10 μm × 10 μm in size. The diameter of the NW was close to the ZnO NW used in LED experiments. One end of the NW was set as the cathode with an Ohmic contact, and the other end was attached to the surface of a p-type thin film component that also serves as a substrate for supporting the NW. The *c*-axis of the NW (its growth direction) was set pointing from the substrate to the cathode. Uniaxial strain was applied along the axis of the NW, and the strain-induced piezoelectric polarization charges existed at the p–n junction. In this simulation work, the piezo-phototronic effect under both tensile strain and compressive strain were studied. For a p-type NW/n-type thin film structure, the simulated results could be amended to apply without any subtle change.

As for material choice, ZnO was utilized as the material for both the n-type NW and the p-type substrate of homojunctions, and p-GaN was utilized to investigate the effect of the p–n heterojunctions.[19] The conclusions from such materials can be easily extrapolated to p-type NWs and other n-type materials. For a simplified model of the phenomenon, strain was set as applied along the *c*-axis growth direction of the NW, the p-type thin film was assumed non-piezoelectric, and factors including spontaneous polarization, deformation potential and reverse piezoelectric effect are neglected here.

The basic material parameters of ZnO/GaN were taken from the database provided with the COMSOL software and from reported data as Table 1.[20,21]

The doping profile of ZnO is set as 1×10^{15} cm^{-3} for both n-type and p-type in our simulation, which is based on the low defect concentration of high-temperature chemical vapor deposition (CVD) synthesized ZnO NWs.[22]

Supporting Information

Supporting Information is available from the Wiley Online Library or from the author. Simulation results for different hole mobility in the p-type area, simulation results for lower p-type doping, simulation results for LED layout in previous experimental reports, simulation results for the influence of electrode layout.

Acknowledgements

This research was supported by U.S. Department of Energy, Office of Basic Energy Sciences (Award DE-FG02–07ER46394), and the "Thousands Talents" program for pioneer researcher and his innovation team, China, Beijing City Committee of Science and Technology projects (Z131100006013004, Z131100006013005).

Received: May 23, 2014
Revised: August 1, 2014
Published online:

[1] Q. Yang, W. H. Wang, S. Xu, Z. L. Wang, *Nano Lett.* **2011**, *11*, 4012.
[2] Z. L. Wang, *Nano Today* **2010**, *5*, 540.
[3] Q. Yang, X. Guo, W. H. Wang, Y. Zhang, S. Xu, D. H. Lien, Z. L. Wang, *ACS Nano* **2010**, *4*, 6285.

[4] M. R. Yang, C. C. Tsai, C. S. Hong, S. Y. Chu, S. L. Yang, *J. Appl. Phys.* **2010**, 108.
[5] C. F. Pan, S. M. Niu, Y. Ding, L. Dong, R. M. Yu, Y. Liu, G. Zhu, Z. L. Wang, *Nano Lett-* **2012**, *12*, 3302.
[6] C. F. Pan, L. Dong, G. Zhu, S. M. Niu, R. M. Yu, Q. Yang, Y. Liu, Z. L. Wang, *Nat. Photonics* **2013**, *7*, 752.
[7] Q. Yang, Y. Liu, C. F. Pan, J. Chen, X. N. Wen, Z. L. Wang, *Nano Lett.* **2013**, *13*, 607.
[8] Y. Zhang, G. Y. Gao, H. L. W. Chan, J. Y. Dai, Y. Wang, J. H. Hao, *Adv. Mater.* **2012**, *24*, 1729.
[9] Y. Liu, Q. Yang, Y. Zhang, Z. Y. Yang, Z. L. Wang, *Adv. Mater.* **2012**, *24*, 1410.
[10] Y. Zhang, Y. Liu, Z. L. Wang, *Adv. Mater.* **2011**, *23*, 3004.
[11] S. M. Sze, K. K. Ng, *Physics of Semiconductor Devices*, Wiley-Interscience, Hoboken, NJ, USA **2007**.
[12] J. Joo, B. Y. Chow, M. Prakash, E. S. Boyden, J. M. Jacobson, *Nat. Mater.* **2011**, *10*, 596.
[13] S. M. Niu, Y. F. Hu, X. N. Wen, Y. S. Zhou, F. Zhang, L. Lin, S. H. Wang, Z. L. Wang, *Adv. Mater.* **2013**, *25*, 3701.
[14] K. Chakrabarty, S. N. Singh, *Solid-State Electron.* **1996**, *39*, 577.
[15] W. S. Yun, J. J. Urban, Q. Gu, H. Park, *Nano Lett.* **2002**, *2*, 447.
[16] J. F. Scott, *Science* **2007**, *315*, 954.
[17] S. O. Kasap, *Optoelectronics and Photonics: Principles and Practice*, Pearson, Boston, MA, USA, **2013**.
[18] M. C. Jeong, B. Y. Oh, M. H. Ham, J. M. Myoung, *Appl. Phys. Lett.* **2006**, *88*.
[19] S. N. Mohammad, A. A. Salvador, H. Morkoc, *Proc. IEEE* **1995**, *83*, 1306.
[20] A. Janotti, C. G. Van de Walle, *Rep. Prog. Phys.* **2009**, *72*.
[21] C. I. Wu, A. Kahn, *J. Appl. Phys.* **1999**, *86*, 3209.
[22] Z. W. Pan, Z. R. Dai, Z. L. Wang, *Science* **2001**, *291*, 1947.

Adv. Mater. **2014**,
DOI: 10.1002/adma.201402328